Differences in Dynamic Structure of LC8 Monomer, Dimer, and Dimer−Peptide Complexes[†]

Justin Hall, Andrea Hall, Nathan Pursifull, and Elisar Barbar*

Department of Biochemistry and Biophysics, Oregon State University, Corvallis, Oregon 97331

Received June 10, 2008; Revised Manuscript Received September 22, 2008

ABSTRACT: Dimerization of dynein light chain LC8 creates two symmetric grooves at the dimer interface with diverse binding capabilities. In addition to pH and protein concentration, dimerization is affected by phosphorylation, as illustrated by a phosphomimetic mutation that promotes dissociation of LC8 to a monomer and subsequent dissociation from the dynein complex *in vitro*. In this work we characterize the dynamic structure and unfolding profiles of an LC8 mutant, H55K, as a model for monomeric LC8 at neutral pH. Backbone ^{15}N relaxation experiments show that the monomer, while primarily ordered, has more heterogeneous dynamics relative to the LC8 dimer, predominantly in residues that ultimately form the binding groove, particularly those in β_1 and β_3 strands. This heterogeneity suggests that conformations that are primed for binding are sampled in the inactive monomer and favored in the active dimer. Further changes of LC8 backbone dynamics upon binding to short peptides from Swallow (Swa) and dynein intermediate chain (IC) were elucidated. The conformational heterogeneity apparent in the LC8 dimer is retained in LC8/IC but is lost in LC8/Swa, suggesting that the degree of ordering upon binding is ligand dependent. The reduced complexity of motion in LC8/Swa correlates with the less favorable entropy of binding of LC8 to Swa relative to IC. We propose that the conformational motility of β_3 has functional significance in dimerization and in ligand binding. In the latter, β_3 flexibility apparently accommodates different binding modes for different ligands resulting in ligand-specific conformational dynamics of the binding site that may impact other processes such as accessibility to phosphorylation.

Dynein light chain LC8[1] (also referred to as DYNLL) was first discovered as an essential component of the microtubule-based molecular motor dynein (*1*) and as such is involved in fundamental processes associated with retrograde trafficking. As a component of the dynein complex, LC8 associates directly with dynein intermediate chain (IC) (*2, 3*). A large fraction of LC8, however, is not associated with dynein (*1*), suggesting alternate functions for LC8 independent of its function in dynein. LC8 interacts with non-dynein proteins in diverse systems, including neuronal nitric oxide synthase, nNOS (*4*), the proapoptotic Bcl2 family protein Bim (*5*), Swallow protein which is involved in bicoid mRNA localization in *Drosophila* (*6, 7*), the rabies virus phosphoprotein (*8*), and Nup159 of the nuclear-pore complex in yeast (*9*). Based on the diversity of these interactions, and the fact that all known LC8 binding partners share a common binding groove on LC8 with the dynein intermediate chain (*10*−*13*), we have proposed that the wide array of LC8 binding partners reflects its role as an essential hub protein (*14*). In this capacity, LC8 functions not simply as a dynein cargo adaptor, as more widely viewed, but as a promoter of dimerization of its monomeric, partially disordered binding partners (*6, 15, 16*).

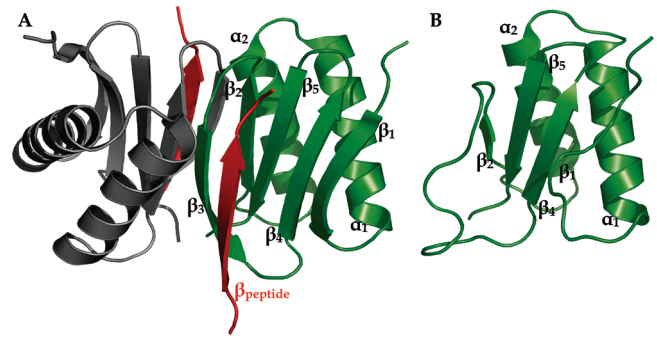

FIGURE 1: Ribbon diagram of (A) dimeric LC8 bound to Swa peptide with the two protomers shown in gray and green and Swa peptide in red ($\beta_{peptide}$) and (B) pH 3 monomer of LC8. Secondary structure elements are labeled. For the pH 3 monomer, β_1 and β_2 are much shorter and β_3 is disordered. Images were produced with PyMol (*52*) using PDB codes 2P1K and 1RHW for LC8/Swa and pH 3 monomer, respectively.

LC8 is an 89 amino acid homodimer (*12*) with each protomer composed of a β-sheet packed against two helices. In the dimer structure complexed with the consensus peptide of a binding partner (Figure 1, left) (*10, 12, 13*), each five-stranded β-sheet includes one strand (β_3) that is contributed by the other protomer. The two β_3 strands are at the

[†] This work is supported by NSF CAREER Grant MCB-0417181 and a Provost undergraduate fellowship for N.P.

* Corresponding author. Tel: 541-737-4143. Fax: 541-737-0481. E-mail: barbare@science.oregonstate.edu.

[1] Abbreviations: LC8, 10 kDa dynein light chain; H55K and S88E, LC8 mutants with His 55 changed to Lys and Ser 88 changed to Glu, respectively; Bim, peptide corresponding to residues 48−64 from proapoptotic Bcl2 family protein; IC, peptide corresponding to residues 123−138 of cytoplasmic dynein intermediate chain; Swa, peptide corresponding to residues 281−297 from Swallow protein; CaM, calmodulin; CD, circular dichroism; HSQC, heteronuclear single-quantum correlation; NOE, nuclear Overhauser effect; H/D, hydrogen/deuterium exchange; H/H, hydrogen/hydrogen exchange; ITC, isothermal titration calorimetry; DSS, 2,2-dimethylsilapentane-5-sulfonic acid; DTT, dithiothreitol; GdnCl, guanidinium chloride.

10.1021/bi801093k CCC: $40.75
Published on Web 10/23/2008

Bim_{48-64} MSCD**KSTQT**PSPPCQAF

$IC_{123-138}$ KETIVYT**KQTQT**TSTG

$Swa_{281-297}$ MYHIRSATSA**KATQT**DF

FIGURE 2: Amino acid sequences of Bim, IC, and Swa peptides with the KXTQT motif in bold and the segment that forms a $\beta_{peptide}$ underlined.

protomer−protomer interface where they form the symmetrical binding grooves of the dimer. Binding of ligands to LC8 dimer involves residues in the binding grooves, primarily those of the β_3 strands. Interestingly, binding leads to further extension of the same β-sheet, as the recognition sequence of the binding partner ($\beta_{peptide}$ in Figure 1) forms a sixth strand. Sequence analyses of the binding partners show that they are intrinsically disordered in the vicinity of their recognition sequence (*14*), suggesting that disorder in these partners may underlie the pleiotropic binding of LC8. Binding is accompanied by disorder to order transition as the ligand partner forms a β-strand ($\beta_{peptide}$). Dissociation of the LC8 dimer at low pH (*17*) eliminates the requisite groove at the dimer interface by disrupting the two β_3 strands (Figure 1B) and thereby prevents binding to IC and other LC8 partners that interact in the groove (*18, 19*).

Phosphorylation of LC8 at Ser 88 is proposed to be involved in vesicle formation, trafficking functions, and cell survival (*20*). The interaction of phosphorylated LC8 with the apoptotic protein Bim is abolished, resulting in reduced apoptosis specifically in human breast cancer cells (*20, 21*). Experiments with a phosphomimetic Ser 88 to Glu (S88E) mutant suggest that phosphorylation acts *in vitro* as a molecular switch by promoting dissociation of the LC8 dimer and subsequent dissociation from dynein (*21*). The phosphomimetic mutant S88E does not bind Bim *in vitro* and *in vivo* (*20*), corroborating the idea that phosphorylation results in an inactive LC8 monomer that does not bind any ligand that occupies the binding grooves at the dimer interface.

Interactions involving the β_3 strands are crucial for stabilizing both the dimer and the LC8/target interfaces and, therefore, play primary roles in both regulation of activity and binding diversity. To investigate both processes, we focus on changes in the structure and dynamics of β_3 strands upon LC8 dimer dissociation and upon LC8/target complex formation. Our model for phosphorylated LC8 monomer at neutral pH is the mutant H55K which is a pure monomer at high protein concentration (*21, 22*). The single mutation of a buried histidine at position 55 at the dimer interface is sufficient to dissociate the dimer at physiological pH (*23*).

In this work we examine the structure and dynamics of the β_3 region in the model LC8 monomer (H55K) which mimics the biologically relevant phosphorylated form, in LC8 dimer, and in complexes of LC8 dimer bound to consensus peptides of LC8 partners (Figure 2). The results support a critical role of β_3 flexibility in the molecular level functioning of LC8. We find that, in solution, residues of the β_3 strand in apo-LC8 dimer (no bound ligand) are highly flexible, even though these residues are organized into the β-sheet in the apo-LC8 dimer NMR (*13*) and crystal (*16*) structures. The thermodynamics of LC8 binding to three peptides and the dynamics of the LC8−peptide complexes reveal a correlation between the flexibility of the binding groove and the entropic cost of binding and demonstrate that the change in flexibility of LC8 is ligand-dependent.

METHODS

Protein Preparation. Both unlabeled and uniformly ^{15}N- or $^{15}N/^{13}C$-labeled LC8 and H55K were prepared from *Drosophila* gene products following methods described earlier (*18*). Purity of >95% was verified by SDS−PAGE and analytical size exclusion chromatography.

Synthetic peptides (Biosynthesis Inc., Lewisville, TX) corresponding to Bim residues 48−64 (Bim), intermediate chain residues 123−138 (IC), and Swallow residues 281−297 (Swa) (Figure 2) were purified by high-performance liquid chromatography on a YMC C-18 column in 0.1% trifluoroacetic acid with a linear gradient (10−30%) of acetonitrile with Bim, IC, and Swa elution at 25%, 15%, and 20%, respectively. Purity and molecular weight were verified by MALDI-TOF mass spectrometry: Bim: 1827.9 Da (1828.0 Da theoretical), IC: 1786.1 Da (1785.9 Da theoretical), and Swa: 1928.1 Da (1928.1 Da theoretical).

Unfolding Studies. CD experiments were conducted on a JASCO 715 spectropolarimeter in a 1 mm cell for a protein concentration of 14 μM in 10 mM sodium phosphate buffer, 0.1 M NaCl, and 5 mM TCEP at pH 7. Data were acquired at 30 °C following procedures and experimental conditions published elsewhere (*17*). Intrinsic fluorescence emission spectra of the single tryptophan residue were determined on a Jobin Yvon/Spex spectrofluorometer at 30 °C.

The denaturation curves were analyzed using a two-state unfolding model (*24*−*26*):

$$M \overset{K_u}{\leftrightarrow} U \tag{1}$$

where M and U are the folded and unfolded monomer, respectively. The two-state process was modeled by calculation of K_u and $\Delta G°$ at each point in the unfolding transition phase. K_u was calculated using eqs 2 and 3:

$$K_u = \frac{[U]}{[M]} = \frac{f_u}{1 - f_u} \tag{2}$$

$$f_u = \frac{y_m - y}{y_m - y_u} \tag{3}$$

where f_u is the fraction of unfolded protein and y_m and y_u are the observed spectroscopic signals for folded and unfolded monomer, respectively. $\Delta G°$ was calculated as $-RT$ ln K_u, and linear extrapolation of $\Delta G°$ to 0 M guanidinium chloride (GdnCl) gives $\Delta G°_{H_2O}$, the free energy of unfolding under standard conditions. The midpoint of the transition (C_m) was determined using the relation $C_m = \Delta G°_{H_2O}/m$. The fits were performed using a χ^2 procedure implemented in Microsoft Excel.

NMR Spectroscopy. All NMR spectra were collected on a 600 MHz Bruker DRX spectrometer. LC8 and H55K samples were prepared at 1 mM protein concentration in 50 mM sodium phosphate and 50 mM sodium chloride at pH 6.7 and contained 1 mM DTT, maleic acid, sodium azide, protease inhibitor cocktail (Roche), 10% (v/v) D_2O, and 3% (v/v) glycerol. Experiments were collected at 30 °C. For LC8 and LC8/peptide comparison experiments, the protein concentration was 1 mM in 50 mM sodium phosphate, 50 mM sodium citrate, and 100 mM sodium chloride at pH 5.5, and experiments were collected at 25 °C. The peptide to protein concentration ratio was greater than 2-fold. The pH was

measured before data acquisition and verified using an internal maleic acid standard. ^{1}H chemical shifts were referenced from an internal DSS signal at 0 ppm (*27*).

^{1}H−^{15}N HSQC spectra were recorded using States−TPPI phase discrimination of 256 increments defined by 128 scans and 1024 points. HNCA and CBCACONH experiments for H55K backbone assignments were performed with 1024 (H), 64 (C), and 20 (N) points. Resonance assignments were deposited in the BMRB with accession number 15953.

R_1, R_2, and steady-state heteronuclear NOE spectra were recorded using the pulse sequence described by Farrow et al. (*28*). R_1 relaxation delays were 0.05, 0.1, 0.15, 0.2, 0.3, 0.5, and 1 s. R_2 relaxation delays were 15.8, 31.7, 63.4, 79.2, 95.0, 126.7, and 142.6 ms. At least one redundant data point was collected for R_1 and R_2 experiments. Steady-state heteronuclear NOE experiments were recorded in the presence and absence of amide proton saturation with 240 complex points. Spectra with proton saturation used a 3 s period of saturation and an additional delay of 1.5 s.

Spectra were processed with NMRPipe (*29*) and analyzed with Burrow-Owl (*30*). Change in ^{1}H−^{15}N HSQC chemical shifts (ΔN−H) between LC8 and H55K was determined using the equation $\Delta N-H = [(\Delta^1H)^2 + (\Delta^{15}N)^2]^{1/2}$ after multiplying the ^{1}H chemical shift by 6.4 (fractional difference in ^{15}N:^{1}H spectral widths) to eliminate ^{15}N chemical shift bias (*31*).

Dynamics Analysis. Peak intensities were measured as peak heights with uncertainty estimated from baseline standard deviation within a 1.4 × 5 ppm rectangle. R_1 and R_2 data were fit using CurveFit version 1.3 (http://www.cum-c.columbia.edu/dept/gsas/biochem/labs/palmer/software/curvefit.html). Errors reported include both uncertainty in the peak height and the error of the exponential fit.

Peak intensities (I) as a function of delay time for R_1 and R_2 were fit to a single exponential $I = I_0 e^{-rate t}$, where I_0 is the peak intensity extrapolated to time 0. NOE values were obtained from the ratios of peak intensities in the presence and absence of amide proton saturation. Uncertainty in the NOE value (σ) was determined using the equation $\sigma/NOE = [(\delta_{unsat}/I_{unsat})^2 + (\delta_{sat}/I_{sat})^2]^{1/2}$, where I and δ correspond to the peak intensity and the baseline noise, respectively.

Backbone amide relaxation parameters were analyzed with the extended Lipari−Szabo formalism (*32, 33*) using the program TENSOR2 (*34*) to assess global tumbling and internal motions. The ^{15}N CSA was set to −170 ppm and the N−H bond length to 1.02 Å. For each data set, a global tumbling correlation time (τ_m) was calculated from the R_2/R_1 ratio of residues assumed to have a negligible exchange contribution to ^{15}N relaxation following the criteria described by Tjandra et al. (*35*). Residues in α_1 commonly failed the acceptance criteria as well as residues 87−89 for all five systems studied. For H55K, LC8, and LC8/IC, additional residues corresponding to the loop connecting α_2/β_2 (51−53), β_3 (61−69), and the loop connecting β_3/β_4 (70−74) were removed from global tumbling calculations, while for LC8/Swa, only residue 62 was additionally omitted. Correlation times and rotational diffusion parameters were determined using Gaussian Monte Carlo simulations.

Internal motions were determined using Monte Carlo sampling methods and *F*-tests validation incorporated in TENSOR2 (*34*). Five standard models were used to describe internal mobility with motion complexity increasing with model number. Model 1 motion is described by S^2; model 2 by S^2 and τ_e; model 3 by S^2 and R_{ex}; model 4 by S^2, τ_e, and R_{ex}; model 5 by S^2, S_f^2, and τ_s. S^2 is the order parameter and describes the amplitude of the N−H vector motion on the nanosecond to picosecond time scale, τ_e is the effective correlation time for the internal motions, and R_{ex} describes slow chemical exchange type motions on the millisecond to microsecond time scale (*36*). A model for the internal motions was rejected if the experimental χ^2 value was higher than the simulated χ^2 value at the 90% confidence limit. Residues in H55K, LC8, LC8/IC, and LC8/Swa that were not adequately fit by any of the five models were omitted from further analysis. For anisotropic analyses, PDB codes 1RHW (*18*), 2P2T (*10*), and 2P1K (*10*) were used for H55K, LC8/IC, and LC8/Swa, respectively, and a recent apo-LC8 crystal structure was used for the LC8 dimer (PDB code 3BRI) (*16*). To check for bias introduced from the structure, H55K, apo-LC8, and LC8/IC were reanalyzed using alternate structures: a single chain from the dimeric LC8 crystal structure (PDB code 3BRI) for H55K, the NMR dimer structure (PDB code 1F3C) (*13*) for apo-LC8, and the LC8/Swa structure (PDB code 2P1K) (*10*) for LC8/IC. For all cases the resultant D_{ratio} ($D_\parallel/D_\perp$), calculated global tumbling time, and internal motions were the same within error as the values obtained using original structures (data not shown).

H/D and H/H Exchange. Hydrogen/deuterium exchange (H/D) experiments for H55K and LC8 were collected at 25 °C in 50 mM sodium phosphate, 50 mM sodium citrate, and 100 mM sodium chloride at pH 5.5. Samples prepared for H/D were flash frozen and lyophilized prior to addition of 100% D_2O. ^{1}H−^{15}N HSQC spectra were collected continuously for the first 18 h and then once every day for 14 days. The dead time of the experiment, defined as time between first exposure to D_2O and the middle of the first HSQC experiment, was 30 min. Peak intensities as a function of time were fit to $I = I_0 e^{-kt} + \Omega$, where t is the time following deuteration, k is the exchange rate, and Ω is a correction factor for baseline distortion and residual H_2O in the sample.

Hydrogen/hydrogen (H/H) exchange spectra for H55K, LC8 dimer, and LC8/Swa were collected using the CLEAN-EX-PM-FHSQC pulse sequence (*37*) at 30 °C in 50 mM sodium phosphate and 50 mM sodium chloride at pH 6.7 with a mixing time of 20 ms.

Isothermal Titration Calorimetry. Bim, IC, and Swa peptides and LC8 were prepared in buffer containing 50 mM sodium phosphate, 50 mM sodium citrate, 100 mM sodium chloride, and 1 mM sodium azide at pH 5.5. The concentration of Bim was determined by weight of dry peptide on a CAHN 25 automatic elecrobalance, accurate to one-thousandth of a milligram. The concentrations of IC and Swa were determined using a sequence-based calculated ϵ_{280} of 1490 $M^{-1}\cdot cm^{-1}$. The concentration of LC8 was determined using ϵ_{280} of 13370 $M^{-1}\cdot cm^{-1}$.

Thermodynamics of binding were obtained using a VP-ITC isothermal titration calorimeter from MicroCal (Northampton, MA). Data were processed using the software package Origin 7.0 (OriginLab Corp., Northampton, MA). For each experiment, an initial injection of 2 μL was performed followed by 27 injections of 10 μL with a 300 s equilibration time between injections. The heat of dilution determined from titrating peptide into buffer at 30 and 35 °C was subtracted from the binding data prior to data fitting.

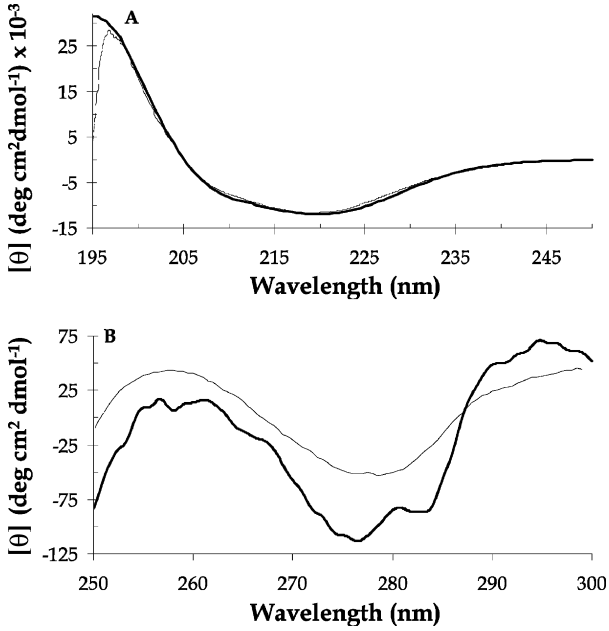

FIGURE 3: (A) Far- and (B) near-UV CD spectra of H55K (light) and WT LC8 (dark). Data were collected at pH 7.0 and monomeric protein concentration of 14 μM for both proteins.

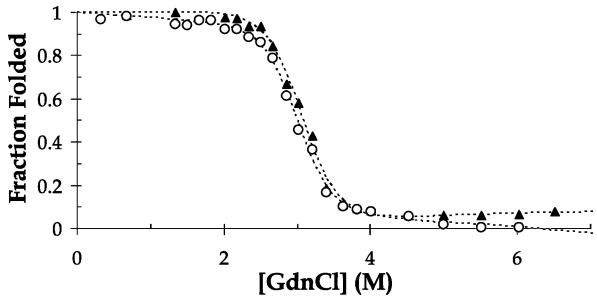

FIGURE 4: GdnCl unfolding profiles of H55K. Loss of intensity in far-UV CD spectra was monitored at 222 nm (circles) and loss of fluorescence intensity was monitored at 327 nm (triangles). Protein concentration was 14 μM for both experiments. Data were acquired at pH 7 and 30 °C using a batch-type experiment to ensure that equilibrium was achieved before data acquisition. A 2-state unfolding model best fits the data (dashed line).

The stoichiometric number (n) was 1.00 ± 0.08 for all experiments using a syringe/cell concentration of 0.5/0.03 mM. The "c value" ($c = [\text{protein}]_{\text{sample cell}} \times K_d^{-1}$) was within the 5−500 value required for reliable determination of association constants (*38*). The error reported is based on deviation from the theoretical best fit.

RESULTS

Stability and Two-State Unfolding of H55K. Far-UV CD (Figure 3) and fluorescence spectra (data not shown) of H55K are similar to those of the WT LC8 dimer, indicating that there is no measurable change upon dissociation of CD-detected secondary structure and of Trp 54 local packing. Near-UV CD spectra, dominated by the signal of Tyr 65 at the dimer interface (*17*), are different (Figure 3B) as expected, consistent with dimer dissociation.

Unfolding profiles for monomeric H55K followed by changes in both fluorescence and far-UV CD at increasing GdnCl concentration are similar (Figure 4), suggesting a two-state unfolding transition. Similar thermodynamic parameters were obtained using a two-state unfolding model for fitting both data sets (Table 1). Equilibrium denaturation experiments carried out over the protein concentration range of 0.4−14 μM show similar unfolding profiles, consistent with H55K being a pure monomer (data not shown).

Table 1: Thermodynamic Parameters Obtained from Equilibrium Denaturation of H55K at pH 7

	$\Delta G°$ (kcal·mol^{-1})	C_m (M)	slope (kcal·mol^{-1}·M^{-1})
CD	7.80	2.99	−2.61
fluorescence	7.45	3.06	−2.44

NMR Structural Characterization of H55K. Resonance assignments of H55K were determined for residues 3−89 from analysis of 3D experiments collected on uniformly ^{15}N- and ^{13}C-labeled protein (Figure 5A). Comparison of the N, H, Cα, and Cβ chemical shifts between H55K and LC8 shows that the largest changes occur for residues 55 through 74 and for residue 88 (Figure 5B−D). In the dimer, these residues primarily correspond to β_3 (residues 63−67), which aligns antiparallel to the opposing protomer's β_2 (residues 53−58). Thus, dissociation of the LC8 dimer results in small changes in chemical shifts for residues in β_2 and large changes for residues in β_3. The change in residue 88 is attributed to being buried at the dimer interface and fully solvent exposed in the monomer.

Dynamics of H55K and Comparison to WT LC8 Dimer. Backbone relaxation dynamics were measured from ^{15}N R_1, R_2, and steady-state heteronuclear NOEs for H55K and dimeric LC8 at similar solution conditions (Figure 6). For H55K, the average R_1 rate is 2.0 s^{-1} with the largest deviation for residues 4−6, 35, 36, and 62−73. The average R_2 rate is 11.3 s^{-1} with the largest deviation for residues 9, 35, 36, and 62−74. The average NOE value is 0.78 with the largest deviation for residues 4−6 and 62−73. Deviation from the average dynamics behavior in H55K is clearly reflected in R_2/R_1 ratios for residues 9, 10, 64, 70, and 74. Except for residues 73 and 74, dimeric LC8 shows more homogeneous dynamics.

Relaxation data were analyzed using the axially symmetric anisotropic diffusion model (Table 2). A correlation time of 6.36 ns for H55K compared to 10.61 ns for the LC8 dimer is consistent with the smaller size of the monomer. The $D_\parallel/D_\perp$ of LC8 (1.27) is larger than H55K (1.07), indicating that the LC8 dimer is more oblate.

Model-free parameters and model-type distribution are shown in Figure 7 for H55K and LC8 dimer. A higher percentage of residues in H55K were fit by models 3 or 4 than by model 1 (Figure 7A). Two stretches of residues in H55K contain significant R_{ex} terms compared to the average (Figure 7D), suggesting conformational heterogeneity. These include residues 4−13, which correspond to the N-terminus and β_1, and residues 64−74, which correspond to β_3 (disordered in monomer), the loop connecting β_3/β_4, and the first two residues of β_4.

Residues in LC8 dimer were fit primarily by models 1 and 3. The large R_{ex} term at the N-terminus, β_1, and β_3 regions observed in H55K has decreased significantly in the LC8 dimer. A small R_{ex} term was necessary to improve the fit of some residues, which are distributed across the sequence with the largest corresponding to residue 74 in β_4.

Comparison of S^2 values between H55K and LC8 shows little difference between residues that have ordered secondary

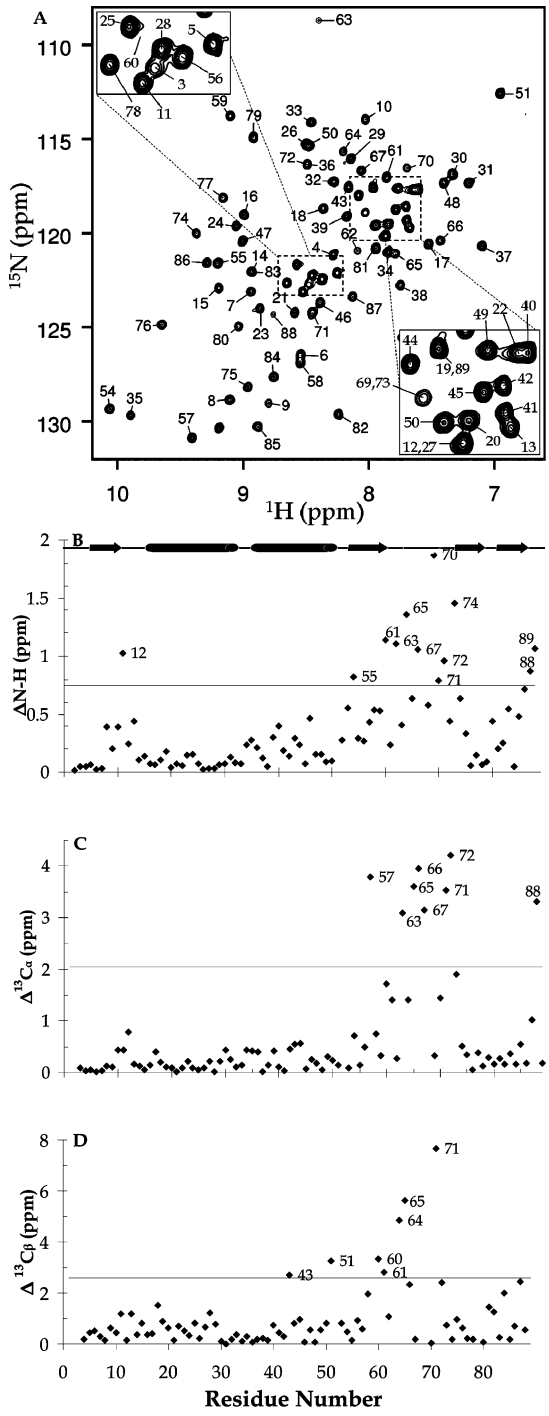

FIGURE 5: NMR analysis of H55K. (A) ^{1}H−^{15}N HSQC spectrum with backbone assignments and absolute (B) ^{1}H−^{15}N, (C) ^{13}Cα, and (D) ^{13}Cβ chemical shift differences between H55K and LC8 are shown. Residues greater than two standard deviations (dashed line) above the average chemical shift difference are labeled. The majority of labeled residues are in the segment which forms β_3 at the dimer interface. The secondary structure of LC8 without β_3 is shown above the plots.

structure elements in LC8, with the exception of β_3. In H55K, the S^2 values for residues 65−73 display significantly lower values than the same residues in the dimer (Figure 7B,F).

Dynamics of LC8/IC and LC8/Swa Complexes. Backbone relaxation dynamics were measured for LC8 and compared to LC8 bound to two KXTQT-motif containing peptides: the intermediate chain residues 123−138 (IC) and the Swallow residues 281−297 (Swa) (Figure 8). The average R_2 values for apo-LC8, LC8/IC, and LC8/Swa are 15.2, 18.1, and 16.9 s^{-1}, respectively. The lower value for apo-LC8 is consistent with its smaller size relative to the complexes, and the lower value for LC8/Swa relative to LC8/IC suggests faster tumbling due to a more compact structure (there is a negligible difference in the size of IC and Swa peptides: Swa is 142 Da greater in mass than IC). Lower R_2 values relative to the average are observed for residues 29−34 and 31−35 for LC8/IC and LC8/Swa, respectively. Both LC8/IC and LC8/Swa have similar average steady-state NOE values with residues 4−6 having the largest deviations from the average. R_2/R_1 average ratio is lower for LC8/Swa relative to LC8/IC and apo-LC8, consistent with more isotropic tumbling and homogeneity of motion in LC8/Swa.

Relaxation data analysis (Table 2) shows that both LC8/peptide complexes have slower tumbling times compared to apo-LC8 of 11.3 ns: 14.1 ns for LC8/IC and 13.2 ns for LC8/Swa. The faster tumbling time of LC8/Swa relative to LC8/IC is consistent with it being more compact. In accord with this, the $D_{\parallel}/D_{\perp}$ of LC8/Swa (1.11) is smaller than that of LC8/IC (1.28), and both are smaller than that of the apo-LC8 dimer (1.39), suggesting that peptide binding results in a more spherical structure.

As with apo-LC8, residues in LC8/IC were mostly fit by models 1 or 3 (Figure 9A,E). A general comparison of the S^2 values, model type, and level of heterogeneous motions in apo-LC8 and LC8/IC suggests a little change in the overall magnitude and type of backbone motions. In contrast, residues in LC8/Swa were fit almost exclusively by model 1, indicating near homogeneous motion for the whole molecule (Figure 9I).

Hydrogen Exchange Measurements. LC8 dimer is more protected from hydrogen exchange than H55K. Eleven amide protons in LC8 and none in H55K have H/D exchange rates that are too slow for accurate determination by H/D experiments under our experimental conditions. There are 41 amide protons in LC8 and 48 in H55K that exchange in the deadtime of the experiment. The additional seven residues in H55K are located at the ends of secondary structure elements of the LC8 dimer. Only residues involved in secondary structure in LC8 have H/D exchange rates measurable in both WT LC8 and H55K under these conditions. Interestingly, residues in β_3 at the dimer interface are *not* protected in the dimer in this time window.

H/H experiments provide exchange rates within the 1−100 ms time scale and are thus complementary to H/D exchange experiments for fast exchanging residues. CLEANEX HSQC spectra for H55K and LC8 are presented in Figure 10. At a 20 ms exchange time, H55K spectra show more peaks corresponding to fast exchanging amide protons consistent with more exposed residues in the monomer. For both proteins, the fast exchanging protons observed in H/H experiments are in the loops and at the ends of secondary structure elements (Figure 11, red). The stretch of residues 63−67 which correspond to β_3, are observed only in the monomer. Only loop residues 61−62 preceding β_3 are observed in the dimer, indicating that residues in β_3 are more protected in the dimer at this time scale and therefore not observed. In the LC8/Swa complex, only residues 3, 4, and 5 at the flexible N-terminus are observed at similar conditions, consistent with diminished flexibility of LC8 upon binding to Swa peptide. Figure 11 summarizes the H/D and

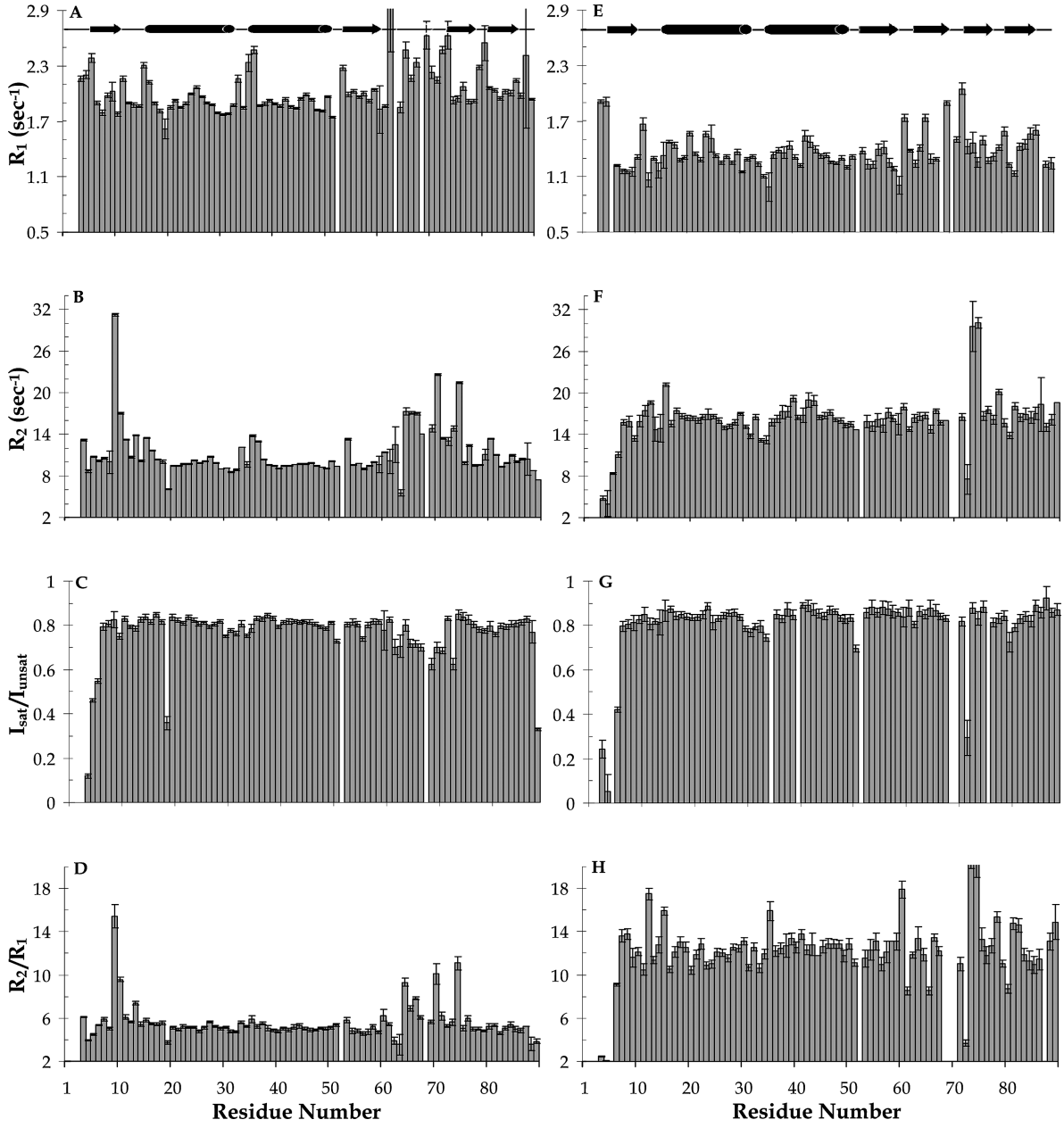

FIGURE 6: Plots of ^{15}N R_1, R_2, and steady-state $^1H-^{15}N$ NOE recorded for H55K (A−C) and LC8 (E−G) at pH 6.7 and 30 °C. R_2/R_1 ratios are shown in (D) and (H) for H55K and LC8, respectively. There is more heterogeneity in R_2 measurements in H55K relative to the LC8 dimer. Protein secondary structure is shown above the plots.

Table 2: Principal Axis Ratios and Axially Symmetric Diffusion Tensor Summary

	principal axis ratio				
protein	I_{xx}	I_{yy}	I_{zz}	τ_m[a] (ns)	D ratio ($D_\parallel/D_\perp$)
H55K	1.00	0.89	0.71	6.36 ± 0.03	1.07
LC8[b]	1.00	0.93	0.52	10.61 ± 0.02	1.27
LC8[c]	1.00	0.93	0.52	11.31 ± 0.07	1.39
LC8/IC	1.00	0.94	0.59	14.07 ± 0.04	1.28
LC8/Swa	1.00	0.93	0.58	13.16 ± 0.06	1.11

[a] Calculated average correlation time. [b] pH 6.7 values. [c] pH 5.5 values.

H/H exchange boundaries mapped onto the structures of monomeric and dimeric LC8.

Thermodynamics of LC8 Binding to Diverse Peptides. Isothermal titration calorimetry (ITC) measurements of LC8 binding to Bim, IC, and Swa peptides performed at 30 and 35 °C show a lower association constant for LC8/IC relative to LC8/Bim or LC8/Swa (Figure 12). Interestingly, while all three peptides share the same binding site on LC8, the thermodynamic parameters governing association are different. At 30 °C, binding to IC is entropically favorable (K_d of 3.0 μM, $\Delta H°$ of −4.0, and $-T\Delta S°$ of −3.8 kcal/mol), while the binding to Bim or Swa is entropically unfavorable (K_d of 0.6 μM, $\Delta H°$ of −10.4 kcal/mol, and $-T\Delta S$ ° of 1.8 kcal/mol for Bim; K_d of 0.6 μM, $\Delta H°$ of −10.7 kcal/mol, and $-T\Delta S°$ of 2.0 kcal/mol for Swa). A similar pattern for thermodynamic parameters is observed at 35 °C (Figure 13).

DISCUSSION

H55K Is a Model for Monomeric LC8 at Neutral pH. H55K is a stable monomer with an average structure similar to one chain of the LC8 dimer as demonstrated by similar CD and fluorescence spectra. Unfolding profiles of H55K show a two-state transition with unfolding free energy of

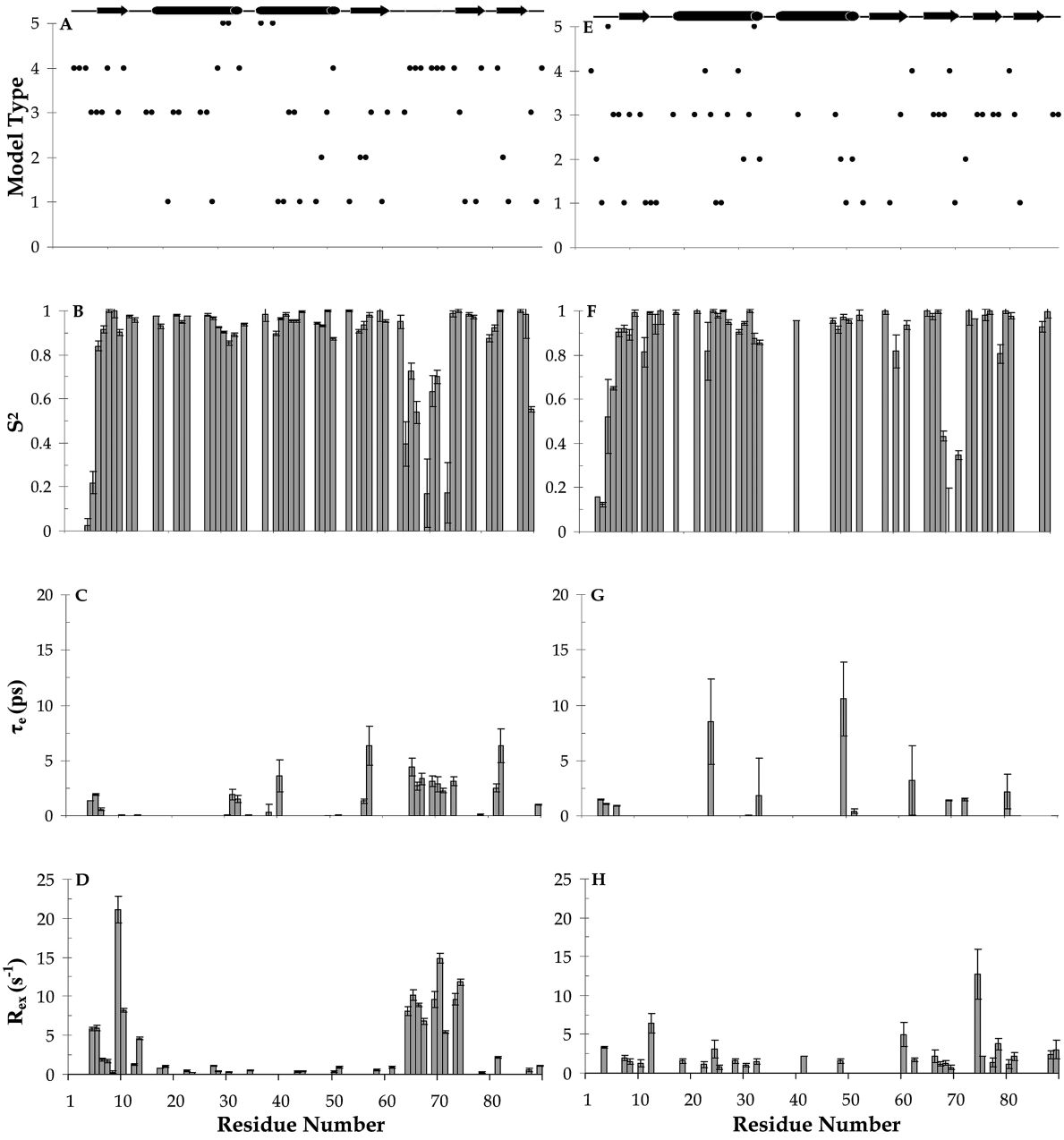

FIGURE 7: Comparison of model-free analysis between H55K (A−D) and LC8 (E−H). Residues in β_3 have lower order parameters (S^2) (B, F) in the monomer relative to the dimer. R_{ex} terms are more prominent in H55K, particularly in residues 9, 10, and 64−74 (D). R_{ex} is distributed along the sequence in LC8 dimer (H).

7.45 kcal/mol. This value is similar to the 7.5 kcal/mol obtained for the monomer unfolding step in the three-state unfolding transition of WT dimeric LC8 at pH 7 (*17*).

The pH 3 WT LC8 is also a stable monomer whose structure is similar to one chain of the LC8 dimer except that β_3 is disordered (Figure 1B) and more flexible than the rest of the protein (*17, 18*). The β_3 strand in H55K is also disordered as indicated by random coil-like secondary chemical shifts and relatively low order parameters. A minor population of ordered conformations for β_1 and β_3, however, is inferred from higher steady-state NOEs and more heterogeneous dynamics than in those observed in the pH 3 WT monomer (*18*). The heterogeneity in residues 62−73 may be partially due to protonated−deprotonated states of His 68 and His 72 as suggested by ref *39* which in H55K have pK_a values of 6.5 and 6.2, respectively (*22*). However, both residues are exposed to solvent in the monomer structure, and therefore we do not anticipate their ionization state to significantly influence conformational heterogeneity. The disorder in β_3 argues against a domain-swapping mechanism of assembly (*18*) since the $\beta_3-\beta_2'$ contacts of the dimer are not replicated in analogous $\beta_3-\beta_2$ contacts in the monomer, as expected for domain swapping (*40*).

The two-state unfolding mechanism for H55K at pH 7 is in contrast to the complex global unfolding profiles reported for the pH 3 WT monomer (*41*). The differences in unfolding mechanisms and backbone dynamics between pH 3 and pH 7 monomers suggest that further unfolding occurs at low pH in addition to dimer dissociation and argue against the suitability of pH 3 WT as a model for monomeric LC8 at neutral pH, as in previous literature (*39, 41−43*).

Heterogeneity in H55K Is Specific to Residues That Form the Binding Groove in the Dimer. Three groups of residues in H55K show nonuniform backbone dynamics at intermedi-

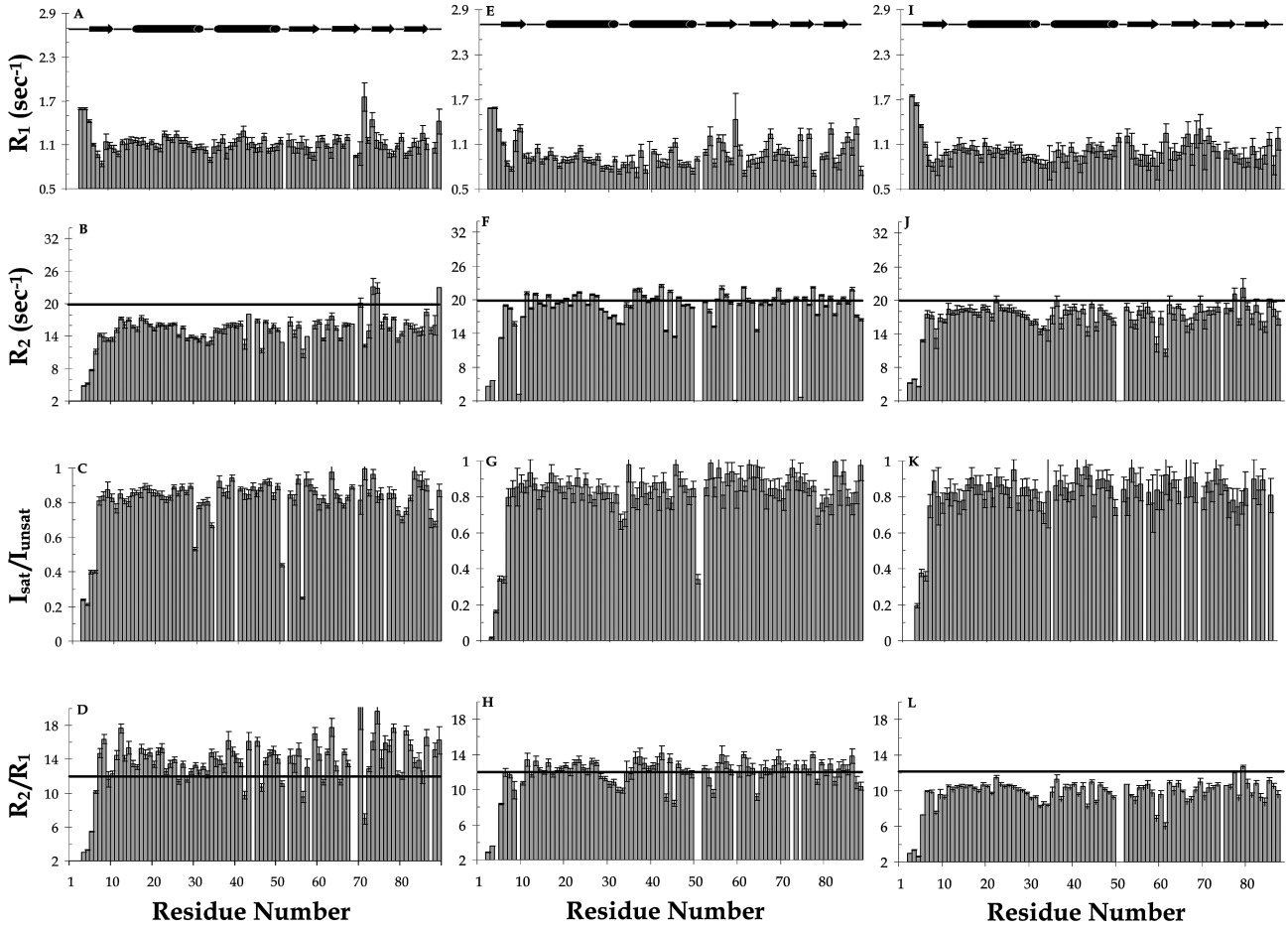

FIGURE 8: Plots of ^{15}N R_1, R_2, and steady-state $^1H-^{15}N$ NOE recorded for apo-LC8 (A−C) LC8/IC (E−G), and LC8/Swa (I−K) at pH 5.5 and 25 °C. R_2/R_1 ratios are shown in (D), (H), and (L) for apo-LC8, LC8/IC, and LC8/Swa, respectively. A line is drawn in (B), (D), (F), (H), (K), and (L) to aid visual comparison. Higher R_2 and R_2/R_1 for LC8/IC indicate more heterogeneous dynamics than for LC8/Swa. Protein secondary structure is shown above the plots.

ate (millisecond to microsecond) and fast (nanosecond to picosecond) time scales: (1) Residues 62−73 exhibit conformational heterogeneity at both the fast time scale (higher R_1, lower steady-state NOE, lower S^2) and intermediate time scale (higher R_2 and higher R_{ex}). (2) Residues 9 and 10 show conformational heterogeneity at the intermediate time scale (higher R_2 and higher R_{ex}). (3) Residues 35 and 36 in the loop connecting helices 1 and 2 show more flexibility at the fast time scale (higher R_1, lower steady-state NOE). In the dimer, while some overall heterogeneity is retained, it is considerably less pronounced than in the monomer.

In crystal structures of LC8 complexes with IC and Swa peptides, residues 9, 35, 36, and 62−73 are directly involved in peptide binding. The side chain of Lys 9 in LC8 makes electrostatic interactions with Asp 296 of Swa. The side chain of Asp 35 and the amide proton of Lys 36 in LC8 form hydrogen bonds with the highly conserved Gln of the KXTQT motif in IC and Swa. Residues 62−73, corresponding to β_3 and the loop connecting β_3/β_4, make direct contacts with the peptide at the dimer interface ($\beta_{peptide}$, Figure 1). Thus, the residues that exhibit heterogeneous backbone dynamics in H55K ultimately form the binding grooves at the dimer interface. These data suggest that in the inactive monomer residues in strands β_1, β_3, and loop β_3/β_4, while on average disordered, also sample a minor population of conformations that are primed for dimerization and ligand binding and are favored upon dimerization.

Hydrogen Exchange Differences upon Dimerization. All residues in β_1 and β_3 in the dimer exchange much faster than the rest of the secondary structure. While the susceptibility to exchange is not surprising for β_1 at the flexible N-terminus, it is surprising for β_3 whose stabilization is inferred from the dimer NMR structure (*13*) and from higher S^2 and steady-state NOE values relative to the monomer (Figures 6 and 7). The apparent mobility of this region in the solution structure is in contrast to the ordered crystal structure. Amide protons of residues 63, 65, and 67 in β_3 and residues 69 and 72 in the loops are completely buried in the crystal structure of the apo-LC8 dimer, and their low temperature factors suggest a high degree of order (*16*). It is possible that the higher H/D exchange rates in β_3 is due to the presence of a minor population of the monomer, which has a disordered β_3 in equilibrium with the dimer. This possibility cannot be ruled out, but lack of protection in β_3 is also observed at neutral pH (*44*) and a high protein concentration where the population of a monomer is minimal (*17, 22*).

While β_3 residues are more flexible by hydrogen exchange criteria than residues in other secondary structure elements in the dimer, they are more ordered than residues in the adjacent loops, residues 61−62 and 69−72. All residues within β_3 have slower exchange rates than those of the same sequence position in the monomer. Taken together, the data at neutral pH suggest that, in the monomer, β_3 is primarily disordered but also samples native-like conformations, while

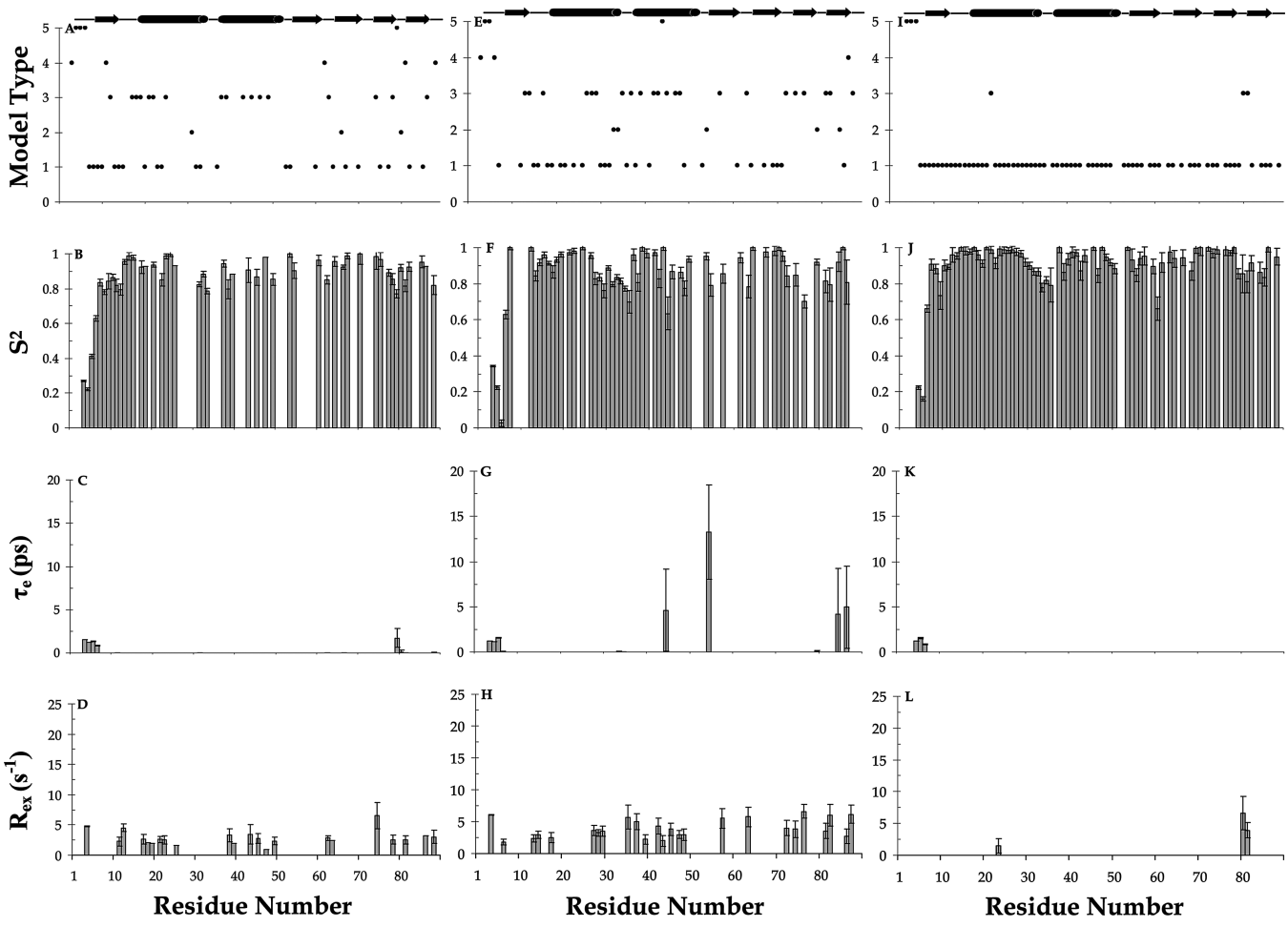

FIGURE 9: Comparison of model-free analysis between apo-LC8 (A, B, C, D), LC8/IC (E, F, G, H), and LC8/Swa (I, J, K, L). Less than half of the residues in apo-LC8 or LC8/IC were adequately fit by model 1, whereas residues in LC8/Swa were fit almost exclusively by model 1, indicating a greater heterogeneity of motion for apo-LC8 (A) or LC8/IC (E) relative to LC8/Swa (I). Loss of the R_{ex} term is observed only with LC8/Swa.

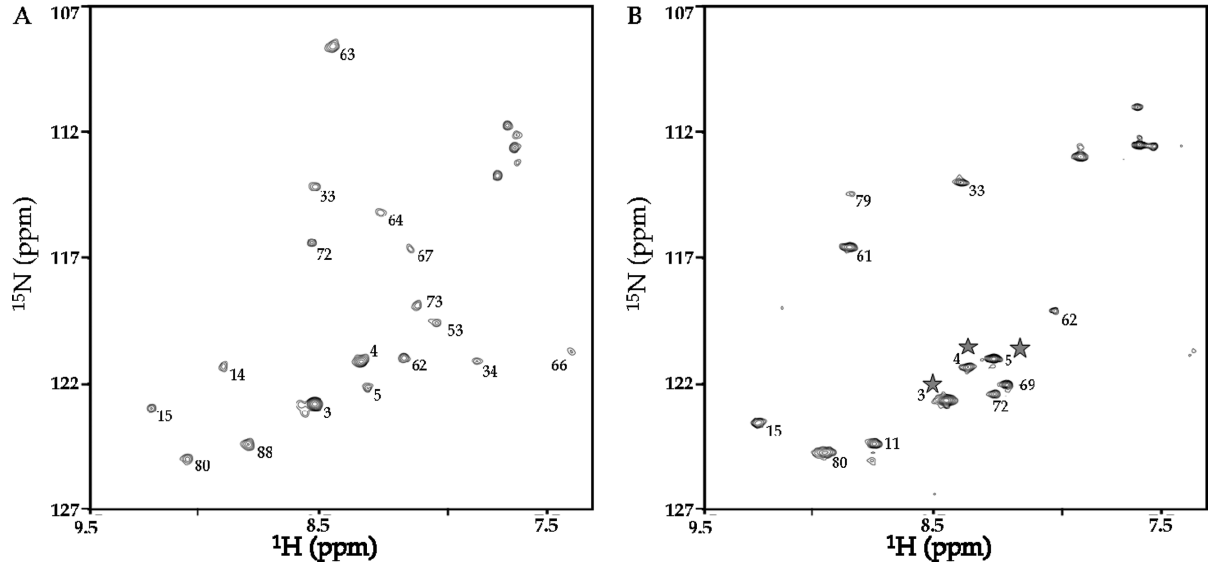

FIGURE 10: $^{1}H-^{15}N$ CLEANEX HSQC spectra for (A) H55K and (B) LC8 collected at pH 6.7 and 30 °C with a mixing time of 20 ms. Peaks shown in the spectra correspond to amide protons that rapidly exchange with water and are colored red on the corresponding structures in Figure 11. Only residues 3, 4, and 5 are observed in LC8/Swa (star).

in the solution dimer, β_3 is primarily native-like but also samples disordered conformations. Further, in the solution dimer, β_3 is apparently more flexible than in either the apo-LC8 dimer crystal structure or the dimer/peptide complex.

Another interesting difference is for Ser 88 which packs against β_3 residues at the dimer interface. The amide NH of Ser 88 shows no protection in H/D exchange in the dimer, exchanges too slow to be observed by H/H exchange in the

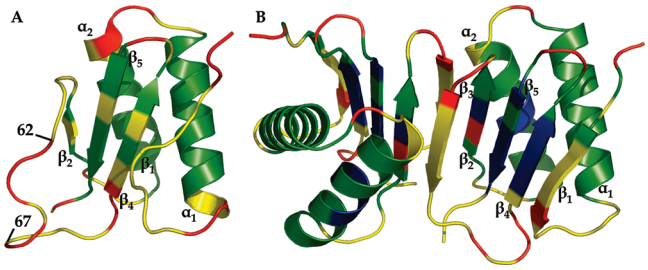

FIGURE 11: Comparison of H/D and H/H exchange between H55K monomer (A) and LC8 dimer (B). The slowest exchanging protons are shown in blue, those that are measured by H/D exchange are shown in green, and the protons that are too fast to measure by H/D exchange but too slow to measure by H/H exchange are shown in yellow. The fastest exchanging protons are shown in red. Images were produced with PyMol using PDB codes 1RHW and 2P1K as models for monomeric and dimeric structures, respectively.

dimer, but exchanges fast enough to be observed by H/H exchange in the monomer. Slowing the exchange of 88 NH in the dimer is consistent with ordering of the interface and possible formation of a transient hydrogen bond as reported in ref *45*.

Changes in Conformational Heterogeneity of LC8 Is Ligand Dependent. Most known LC8 binding partners have either a KXTQT or a less common GIQVD sequence that is considered to be an LC8 binding motif (*3, 46*). In crystal and NMR structures of LC8 with Bim, IC, and Swa peptides, all containing the KXTQT recognition sequence, these ligands share a common site on LC8. The backbone atoms for the bound IC and Swa peptides and the adjacent β_3 from LC8 can be overlaid with an RMSD of 0.2 Å (*10*). Despite average structure similarities, dynamics analysis of LC8 in complex with IC or Swa peptides shows a striking difference in the complexity of motion. These experiments were performed with a large excess of the ligand, at conditions where the protein is >99.9% bound. For both apo-LC8 and LC8/IC, models containing τ_e and R_{ex} parameters are required for more than half of the residues being fit. In contrast, residues in LC8/Swa were analyzed almost exclusively by model 1, consistent with higher homogeneity of motion relative to apo-LC8 or LC8/IC. The difference in complexity of motion suggests a significant ordering of LC8 backbone dynamics only upon binding to Swa.

The greater order in LC8/Swa relative to LC8/IC inferred from backbone relaxation dynamics is consistent with the increased protection from hydrogen exchange observed for LC8/Swa relative to LC8/IC (*10*). ^{15}N backbone dynamics of LC8/Bim reported earlier show that, as with Swa, Bim binding to LC8 causes an increase in the homogeneity of the motion particularly in the binding groove and led to the proposal that the flexibility of the binding grooves in LC8 underlies its binding diversity (*44*). Comparison of the dynamics of LC8 with the three peptide partners suggests that the extent of ordering of the binding groove is not the same for all peptides. There is an increase in homogeneity of the whole protein with Swa and Bim but not with IC. Since all three peptides share the KXTQT recognition motif, residues that flank the recognition motif must dictate the ordering of the groove upon binding.

Correlation between Thermodynamics and Dynamics of Binding. LC8 binds many diverse partners and fits the definition of an ordered hub for disordered partners (*14*). As has been demonstrated for calmodulin, CaM (*47*), another primarily ordered hub protein (*48*), LC8 can bind to a large number of different proteins in the same groove, with roughly the same affinity but with different thermodynamic association parameters. Similar to CaM, the flexibility of the binding groove may allow accommodation of significantly different peptide sequences for high-affinity binding (*44, 49*).

The association between LC8 and IC is entropically favorable, while the association between LC8 and Bim or Swa is enthalpically driven and entropically disfavored. A difference of 5.5 kcal/mol in $T\Delta S°$ between IC and Bim or Swa binding is compensated by a difference of 6.5 kcal/mol in $\Delta H°$ at 30 °C. A recent study by Leung et al. shows that rearrangement of solvent hydrogen bond networks may provide the driving force for nonspecific binding interactions (*50*). In principle, the finding of Leung et al. can be applied to the LC8/ligand system; however, the differences between nonspecific host/guest and a preorganized protein/ligand binding system make it difficult to interpret the magnitude of solvent contributions to the measured LC8/ligand thermodynamic binding parameters.

The LC8/IC and LC8/Swa crystal structures show similar burial of hydrophobic surface area (*10*). Differences in side chain electrostatic interactions are observed in the crystal structures of LC8/IC and LC8/Swa and are consistent with the larger enthalpy of binding for LC8/Swa. Asp 296 of Swa and Lys 9 of LC8 form an electrostatic bridge, which is absent in IC (the corresponding residue in IC is Thr 135). There is also an intrachain hydrogen bond between the carboxyl oxygen of Swa Thr 288 and the side chain of Ser 289, whereas there is no such interaction between the corresponding residues of IC (Val 127 and Tyr 128). Thus the differences in binding enthalpies correlate with electrostatic differences between LC8/IC and LC8/Swa interactions.

^{15}N backbone order parameters are similar for both complexes, but conformational heterogeneity measured as deviations from the simplest model is quite different. The entropically favored IC binding to LC8 shows a minimal change in the backbone dynamics relative to apo-LC8, while the entropically disfavored Swa and Bim binding is consistent with the increase in homogeneous dynamics in LC8/Swa and LC8/Bim relative to both apo-LC8 and LC8/IC. Thus the differences in binding entropies correlate with changes in backbone dynamics occurring upon binding.

Based on the available data it is our conclusion that a significant contribution to the difference in enthalpic and entropic binding energies can be explained by differences in LC8/ligand electrostatics and changes in protein dynamics. As has been observed for CaM association with several of its binding partners (*47*), changes in LC8's internal dynamics are ligand-dependent and illustrate the importance of conformational entropy in high-affinity protein−protein interactions (*47, 49*).

Dynamics and Regulation. In crystal structures of apo-LC8 and LC8/peptide complexes, the side chain of Ser 88 is buried and not apparently accessible to phosphorylation. This raises the question of how Ser 88, the putative phosphorylation site (*51*), becomes phosphorylated in the cell. The studies presented here show an overall conformational heterogeneity in apo-LC8 that is not restricted to the binding groove but spans the sequence and is retained with IC binding but not with Swa binding. This raises the

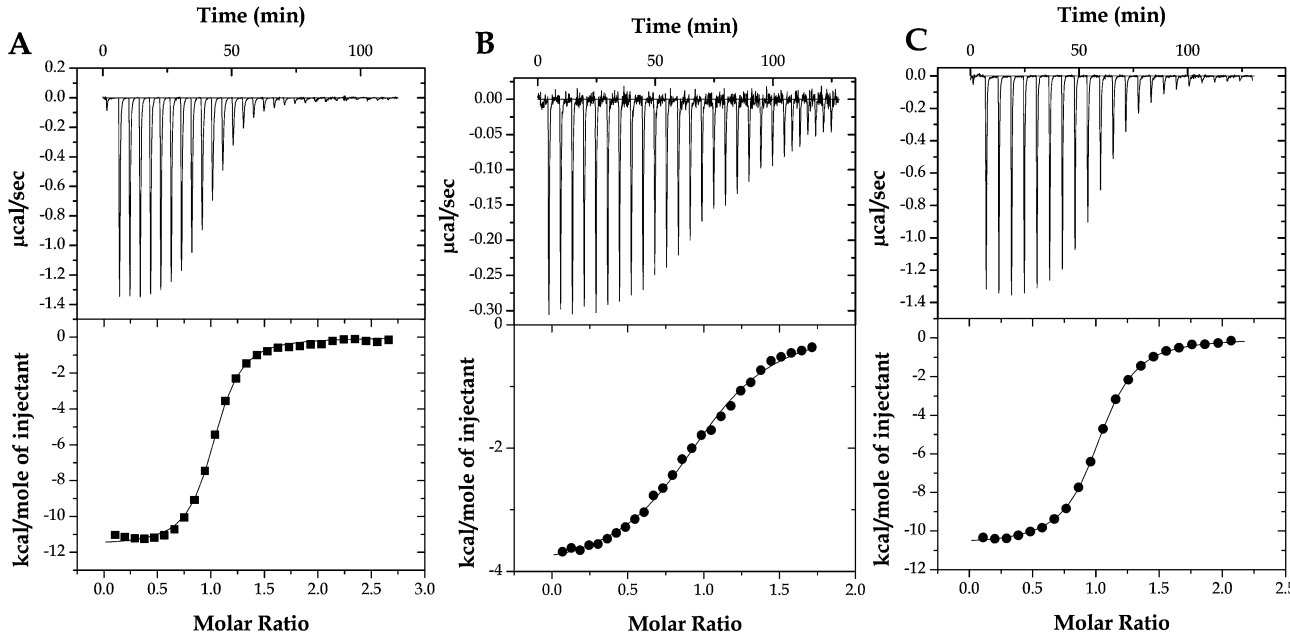

FIGURE 12: ITC raw data (top panels) and binding isotherms (bottom panel) for the titration of LC8 with (A) Bim, (B) IC, and (C) Swa peptides at 30 °C. Solid lines in the bottom charts represent the theoretical fit for the A + B to AB binding model, where A corresponds to the peptide and B corresponds to one protomer of LC8. The transition region of the curves is well fit, indicating accurate determination of association constants. LC8 binds IC with the lowest affinity.

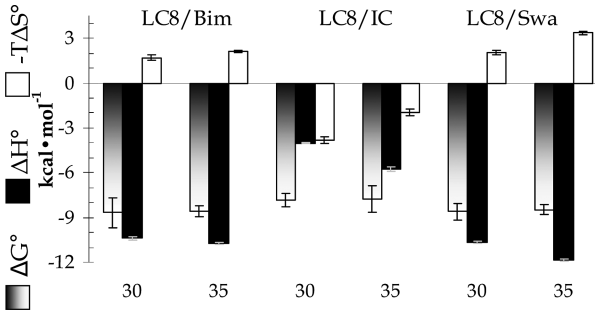

FIGURE 13: Plot of thermodynamic association parameters for LC8/Bim, LC8/IC, and LC8/Swa at 30 and 35 °C. The dissociation constants (K_d) at 30 and 35 °C for LC8/Bim are 0.6 and 0.8 μM, for LC8/IC are 3.0 and 3.3 μM, and for LC8/Swa are 0.6 and 1.0 μM.

possibility that the conformational heterogeneity in apo-LC8 permits transient exposure of the Ser 88 side chain for phosphorylation. Using the same reasoning, it is also possible that the flexibility in the LC8/IC complex is retained to allow phosphorylation in the bound form, while no such regulation may be required for the LC8/Swa or LC8/Bim complexes.

Summary. H55K is a model for monomeric LC8 at neutral pH and shows considerable conformational heterogeneity relative to the pH 3 WT monomer, primarily for residues that ultimately form the binding grooves at the dimer interface. The presence in the monomer of a few mostly disordered residues that sample ordered conformations suggests that dimerization and ligand binding selects for minor populations of native-like conformations in the inactive monomer ensemble. In both the monomer and dimer, β_3 is highly disordered but is nevertheless more ordered on average in the dimer and becomes considerably more ordered in the complex. Upon binding, β_3 makes contacts with the peptide that is itself intrinsically disordered but forms the sixth strand in the complex (*14*), making this an example of two highly flexible segments (β_3 and $\beta_{peptide}$) that fold upon specific binding. Comparison of backbone dynamics between the two bound forms shows a more dynamic fit of IC relative to Swa in the binding groove and suggests that the increase in ordered structure observed in LC8 upon binding is peptide-dependent. The difference in the entropic energetic cost associated with LC8 binding correlates with the large difference in LC8 backbone dynamics upon association with peptide partners and suggests that the conformational entropy of the protein modulates its affinity to diverse ligands. This raises the possibility that there are functional pressures on LC8 to tailor changes in its internal dynamics for different binding partners. Conformational heterogeneity may also underlie selective regulation by phosphorylation.

ACKNOWLEDGMENT

We acknowledge the support of the nucleic acid and protein core and the mass spectrometry facilities and services core in the OSU Environmental Health Sciences Center (NIH/NIEHS 00210). The authors thank Serena Mills and Yujuan Song for sample preparation, Greg Benison for help with NMR data collection and analysis, and the rest of the Barbar laboratory for valuable discussion. The authors gratefully acknowledge advice from Professors Martin Blackledge and Art Palmer regarding model-free analysis.

REFERENCES

1. King, S. M., Barbarese, E., Dillman, J. F., PatelKing, R. S., Carson, J. H., and Pfister, K. K. (1996) Brain cytoplasmic and flagellar outer arm dyneins share a highly conserved M(r) 8,000 light chain. *J. Biol. Chem. 271*, 19358–19366.
2. Makokha, M., Hare, M., Li, M. G., Hays, T., and Barbar, E. (2002) Interactions of cytoplasmic dynein light chains Tctex-1 and LC8 with the intermediate chain IC74. *Biochemistry 41*, 4302–4311.
3. Lo, K. W. H., Naisbitt, S., Fan, J. S., Sheng, M., and Zhang, M. J. (2001) The 8-kDa dynein light chain binds to its targets via a conserved (K/R)XTQT motif. *J. Biol. Chem. 276*, 14059–14066.
4. Jaffrey, S. R., and Snyder, S. H. (1996) PIN: An associated protein inhibitor of neuronal nitric oxide synthase. *Science 274*, 774.
5. Puthalakath, H., Huang, D. C. S., O'Reilly, L. A., King, S. M., and Strasser, A. (1999) The proapoptotic activity of the Bcl-2

family member Bim is regulated by interaction with the dynein motor complex. *Mol. Cell 3*, 287–296.
6. Wang, L., Hare, M., Hays, T. S., and Barbar, E. (2004) Dynein light chain LC8 promotes assembly of the coiled-coil domain of swallow protein. *Biochemistry 43*, 4611–4620.
7. Schnorrer, F., Bohmann, K., and Nusslein-Volhard, C. (2000) The molecular motor dynein is involved in targeting Swallow and bicoid RNA to the anterior pole of Drosophila oocytes. *Nat. Cell Biol. 2*, 185–190.
8. Tan, G. S., Preuss, M. A., Williams, J. C., and Schnell, M. J. (2007) The dynein light chain 8 binding motif of rabies virus phosphoprotein promotes efficient viral transcription. *Proc. Natl. Acad. Sci. U.S.A. 104*, 7229–7234.
9. Stelter, P., Kunze, R., Flemming, D., Hopfner, D., Diepholz, M., Philippsen, P., Bottcher, B., and Hurt, E. (2007) Molecular basis for the functional interaction of dynein light chain with the nuclear-pore complex. *Nat. Cell Biol. 9*, 788–796.
10. Benison, G., Karplus, P. A., and Barbar, E. (2007) Structure and dynamics of LC8 complexes with KXTQT-motif peptides: Swallow and dynein intermediate chain compete for a common site. *J. Mol. Biol. 371*, 457–468.
11. Williams, J. C., Roulhac, P. L., Roy, A. G., Vallee, R. B., Fitzgerald, M. C., and Hendrickson, W. A. (2007) Structural and thermodynamic characterization of a cytoplasmic dynein light chain-intermediate chain complex. *Proc. Natl. Acad. Sci. U.S.A. 104*, 10028–10033.
12. Liang, J., Jaffrey, S. R., Guo, W., Snyder, S. H., and Clardy, J. (1999) Structure of the PIN/LC8 dimer with a bound peptide. *Nat. Struct. Biol. 6*, 735–740.
13. Fan, J. S., Zhang, Q., Tochio, H., Li, M., and Zhang, M. J. (2001) Structural basis of diverse sequence-dependent target recognition by the 8 kDa dynein light chain. *J. Mol. Biol. 306*, 97–108.
14. Barbar, E. (2008) Dynein light chain LC8 is a dimerization hub essential in diverse protein networks. *Biochemistry 47*, 503–508.
15. Nyarko, A., Hare, M., Hays, T. S., and Barbar, E. (2004) The intermediate chain of cytoplasmic dynein is partially disordered and gains structure upon binding to light-chain LC8. *Biochemistry 43*, 15595–15603.
16. Benison, G., Karplus, P. A., and Barbar, E. (2008) The interplay of ligand binding and quaternary structure in the diverse interactions of dynein light chain LC8. *J. Mol. Biol.* (in press).
17. Barbar, E., Kleinman, B., Imhoff, D., Li, M. G., Hays, T. S., and Hare, M. (2001) Dimerization and folding of LC8, a highly conserved light chain of cytoplasmic dynein. *Biochemistry 40*, 1596–1605.
18. Makokha, M., Huang, Y. J., Montelione, G., Edison, A. S., and Barbar, E. (2004) The solution structure of the pH induced monomer of dynein light chain from Drosophila. *Protein Sci. 13*, 727–734.
19. Wang, W., Lo, K. W., Kan, H. M., Fan, J. S., and Zhang, M. (2003) Structure of the monomeric 8-kDa dynein light chain and mechanism of the domain-swapped dimer assembly. *J. Biol. Chem. 278*, 41491–41499.
20. Song, C., Wen, W., Rayala, S. K., Chen, M., Ma, J., Zhang, M., and Kumar, R. (2008) Serine 88 phosphorylation of the 8-kDa dynein light chain 1 is a molecular switch for its dimerization status and functions. *J. Biol. Chem. 283*, 4004–4013.
21. Song, Y., Benison, G., Nyarko, A., Hays, T. S., and Barbar, E. (2007) Potential role for phosphorylation in differential regulation of the assembly of dynein light chains. *J. Biol. Chem. 282*, 17272–17279.
22. Nyarko, A., Cochrun, L., Norwood, S., Pursifull, N., Voth, A., and Barbar, E. (2005) Ionization of His 55 at the dimer interface of dynein light-chain LC8 is coupled to dimer dissociation. *Biochemistry 44*, 14248–14255.
23. Barbar, E., and Hare, M. (2004) Characterization of the cargo attachment complex of cytoplasmic dynein using NMR and mass spectrometry. *Methods Enzymol. 380*, 219–241.
24. Fan, J. S., Zhang, Q. A., Li, M., Tochio, H., Yamazaki, T., Shimizu, M., and Zhang, M. J. (1998) Protein inhibitor of neuronal nitric-oxide synthase, PIN, binds to a 17-amino acid residue fragment of the enzyme. *J. Biol. Chem. 273*, 33472–33481.
25. Cheng, X., Gonzalez, M. L., and Lee, J. C. (1993) Energetics of intersubunit and intrasubunit interactions of Escherichia coli adenosine cyclic 3′,5′-phosphate receptor protein. *Biochemistry 32*, 8130–8139.
26. Santoro, M. M., and Bolen, D. W. (1988) Unfolding free energy changes determined by the linear extrapolation method. 1. Unfolding of phenylmethanesulfonyl alpha-chymotrypsin using different denaturants. *Biochemistry 27*, 8063–8068.
27. Wishart, D. S., Bigam, C. G., Yao, J., Abildgaard, F., Dyson, H. J., Oldfield, E., Markley, J. L., and Sykes, B. D. (1995) ^{1}H, ^{13}C and ^{15}N chemical shift referencing in biomolecular NMR. *J. Biomol. NMR 6*, 135–140.
28. Farrow, N. A., Zhang, O., Forman-Kay, J. D., and Kay, L. E. (1994) A heteronuclear correlation experiment for simultaneous determination of ^{15}N longitudinal decay and chemical exchange rates of systems in slow equilibrium. *J. Biomol. NMR 4*, 727–734.
29. Delaglio, F., Grzesiek, S., Vuister, G. W., Zhu, G., Pfeifer, J., and Bax, A. (1995) NMRPipe: a multidimensional spectral processing system based on UNIX pipes. *J. Biomol. NMR 6*, 277–293.
30. Benison, G., Berkholz, D. S., and Barbar, E. (2007) Protein assignments without peak lists using higher-order spectra. *J. Magn. Reson. 189*, 173–181.
31. Wishart, D. S., Sykes, B. D., and Richards, F. M. (1992) The chemical shift index: a fast and simple method for the assignment of protein secondary structure through NMR spectroscopy. *Biochemistry 31*, 1647–1651.
32. Clore, G. M., Szabo, A., Bax, A., Kay, L. E., Driscoll, P. C., and Gronenborn, A. M. (1990) Deviations from the simple two-parameter model-free approach to the interpretation of nitrogen-15 nuclear magnetic relaxation of proteins. *J. Am. Chem. Soc. 112*, 4989–4991.
33. Lipari, G., and Szabo, A. (1982) Model-free approach to the interpretation of nuclear magnetic resonance relaxation in macromolecules. 1. Theory and range of validity. *J. Am. Chem. Soc. 104*, 4546.
34. Dosset, P., Hus, J. C., Marion, D., and Blackledge, M. (2001) A novel interactive tool for rigid-body modeling of multi-domain macromolecules using residual dipolar couplings. *J. Biomol. NMR 20*, 223–231.
35. Tjandra N., Feller, S. E., Pastor, R. W., and Bax, A. (1995) Rotational diffusion anisotropy of human ubiquitin from ^{15}N NMR relaxation. *J. Am. Chem. Soc. 117*, 12562–12566.
36. Mandel, A. M., Akke, M., and Palmer, A. G., III. (1995) Backbone dynamics of Escherichia coli ribonuclease HI: correlations with structure and function in an active enzyme. *J. Mol. Biol. 246*, 144–163.
37. Hwang, T. L., van Zijl, P. C., and Mori, S. (1998) Accurate quantitation of water-amide proton exchange rates using the phase-modulated CLEAN chemical EXchange (CLEANEX-PM) approach with a Fast-HSQC (FHSQC) detection scheme. *J. Biomol. NMR 11*, 221–226.
38. Turnbull, W. B., and Daranas, A. H. (2003) On the value of c: can low affinity systems be studied by isothermal titration calorimetry? *J. Am. Chem. Soc. 125*, 14859–14866.
39. Mohan, P. M., Barve, M., Chatterjee, A., and Hosur, R. V. (2006) pH driven conformational dynamics and dimer-to-monomer transition in DLC8. *Protein Sci. 15*, 335–342.
40. Schlunegger, M. P., Bennett, M. J., and Eisenberg, D. (1997) Oligomer formation by 3D domain swapping: a model for protein assembly and misassembly. *Adv. Protein Chem. 50*, 61–122.
41. Chatterjee, A., Krishna Mohan, P. M., Prabhu, A., Ghosh-Roy, A., and Hosur, R. V. (2007) Equilibrium unfolding of DLC8 monomer by urea and guanidine hydrochloride: Distinctive global and residue level features. *Biochimie 89*, 117–134.
42. Krishna Mohan, P. M., Barve, M., Chatterjee, A., Ghosh-Roy, A., and Hosur, R. V. (2008) NMR comparison of the native energy landscapes of DLC8 dimer and monomer. *Biophys. Chem. 134*, 10–19.
43. Krishna Mohan, P. M. (2007) Unfolding energetics and conformational stability of DLC8 monomer. *Biochimie 89*, 1409–1415.
44. Fan, J. S., Zhang, Q., Tochio, H., and Zhang, M. (2002) Backbone dynamics of the 8 kDa dynein light chain dimer reveals molecular basis of the protein's functional diversity. *J. Biomol. NMR 23*, 103–114.
45. Mohan, P. M., and Hosur, R. V. (2008) NMR characterization of structural and dynamics perturbations due to a single point mutation in Drosophila DLC8 dimer: functional implications. *Biochemistry 47*, 6251–6259.
46. Rodriguez-Crespo, I., Yelamos, B., Roncal, F., Albar, J. P., Ortiz de Montellano, P. R., and Gavilanes, F. (2001) Identification of novel cellular proteins that bind to the LC8 dynein light chain using a pepscan technique. *FEBS Lett. 503*, 135–141.

47. Frederick, K. K., Marlow, M. S., Valentine, K. G., and Wand, A. J. (2007) Conformational entropy in molecular recognition by proteins. *Nature 448*, 325–329.
48. Dunker, A. K., Cortese, M. S., Romero, P., Iakoucheva, L. M., and Uversky, V. N. (2005) Flexible nets. The roles of intrinsic disorder in protein interaction networks. *FEBS J. 272*, 5129–5148.
49. Lee, A. L., Kinnear, S. A., and Wand, A. J. (2000) Redistribution and loss of side chain entropy upon formation of a calmodulin-peptide complex. *Nat. Struct. Biol. 7*, 72–77.
50. Leung, D. H., Bergman, R. G., and Raymond, K. N. (2008) Enthalpy-entropy compensation reveals solvent reorganization as a driving force for supramolecular encapsulation in water. *J. Am. Chem. Soc. 130*, 2798–2805.
51. Vadlamudi, R. K., Bagheri-Yarmand, R., Yang, Z., Balasenthil, S., Nguyen, D., Sahin, A. A., den Hollander, P., and Kumar, R. (2004) Dynein light chain 1, a p21-activated kinase 1-interacting substrate, promotes cancerous phenotypes. *Cancer Cell 5*, 575–585.
52. DeLano, W. L. (2002) *The PyMOL Molecular Graphics System*, DeLano Scientific, San Carlos, CA.

BI801093K